Reconstruction of tip-surface interactions with multimodal intermodulation atomic force microscopy

Stanislav S. Borysov,[1,2,*] Daniel Platz,[1] Astrid S. de Wijn,[3] Daniel Forchheimer,[1] Eric A. Tolén,[4] Alexander V. Balatsky,[2,5] and David B. Haviland[1]

[1]*Nanostructure Physics, KTH Royal Institute of Technology, Roslagstullsbacken 21, SE-106 91 Stockholm, Sweden*

[2]*Nordita, KTH Royal Institute of Technology and Stockholm University, Roslagstullsbacken 23, SE-106 91 Stockholm, Sweden*

[3]*Department of Physics, Stockholm University, SE-106 91 Stockholm, Sweden*

[4]*Intermodulation Products AB, Vasavägen 29, Solna SE-169 58, Sweden*

[5]*Theoretical Division and Center for Integrated Nanotechnologies, Los Alamos National Laboratory, Los Alamos, New Mexico 87545, USA*

(Received 2 May 2013; published 3 September 2013)

We propose a theoretical framework for reconstructing tip-surface interactions using the intermodulation technique when more than one eigenmode is required to describe the cantilever motion. Two particular cases of bimodal motion are studied numerically: one bending and one torsional mode, and two bending modes. We demonstrate the possibility of accurate reconstruction of a two-dimensional conservative force field for the former case, while dissipative forces are studied for the latter.

DOI: 10.1103/PhysRevB.88.115405 PACS number(s): 68.37.Ps, 05.45.−a, 62.25.−g

I. INTRODUCTION

Atomic force microscopy[1] (AFM) has become one of the most important tools for the study of nanometer-scale surface properties of a wide range of materials. The initial goal of AFM was surface topography imaging which was performed by scanning a cantilever with a sharp tip over a surface while keeping its deflection constant. It was later realized that the reconstruction of tip-surface interactions was possible and that these interactions contain valuable information about material properties.[2,3] One of the first reconstruction methods was based on measurement of the quasistatic bending of the cantilever beam as its base was slowly moved toward and away from the surface. Two drawbacks of this method are the slow speed of measurement and the lack of ability to reconstruct dissipative forces which are always present in tip-surface interactions due to nonelastic deformations of the sample, breaking chemical bonds, or other irreversible processes.[4–8]

The development of dynamic AFM opened new pathways for a more profound study of tip-surface interactions. In dynamic AFM the cantilever is treated as an underdamped oscillator (high Q factor) driven at a resonance where the response to external forces is enhanced by a factor Q. A variety of methods for determining the tip-surface interaction have been devised,[9–15] some making use of amplitude or frequency modulation.[16–25] In this paper we consider intermodulation AFM (ImAFM)[26] which can rapidly extract a large amount of information about tip-surface interactions in a relatively simple and convenient way.[27,28] With ImAFM we have the possibility of high resolution surface property mapping at interactive scan speeds and reconstruction of the tip-surface interaction at each pixel.

The main idea underlying ImAFM is to use the nonlinear tip-surface forces to create high-order intermodulation of discrete tones in a frequency comb.[29] The method can be generally applied to any resonator subject to a nonlinear force when it is driven with at least two frequencies ω_{d1} and ω_{d2}. Nonlinear response in the frequency domain occurs not only at the drive frequencies and their harmonics $n\omega_{d1}$ and $m\omega_{d2}$, where n and m are integers, but also at their linear combinations $n\omega_{d1} + m\omega_{d2}$ or intermodulation products. Due to the signal enhancement near resonance and finite detection noise in measurement, a typical spectrum of cantilever motion can be obtained only in a narrow frequency band near a resonance. Concentrating as many intermodulation products as possible close to a resonance results in more information for reconstruction of the nonlinear forces (Fig. 1).

The sensitivity enhancement of dynamic AFM occurs not only at one single eigenmode, but at several eigenmodes simultaneously. Measurement of the sample response at higher frequencies is reported to improve contrast when imaging and enable material property measurements.[30–36] If we also excite a torsional resonance of the cantilever we open up the possibility of measuring lateral forces acting on the tip.[37–39] Additionally, when driving the cantilever at more than one eigenmode, new frequency bands become available for collecting intermodulation products, resulting from the nonlinear force which couples multiple eigenmodes.[40] While ImAFM has been well studied for the case of one flexural mode,[27,28,41–43] the multi-eigenmode problem remains open. In the current investigation we explore the possibility of reconstructing two-dimensional tip-surface force fields using bimodal tip motion in one dimension (exciting two flexural modes) as well as in two dimensions (exciting one flexural and one torsional mode).

The paper is organized as follows: in Sec. II we consider general properties of the cantilever model and tip-surface interactions. In Sec. III we recount the basic principles of ImAFM, demonstrate how to obtain intermodulation spectra of tip-surface forces, and develop an extension of the spectral fitting method[27,28] of force reconstruction for the multimodal case. In Sec. IV numerical results for the reconstruction of two-dimensional conservative and dissipative forces are presented. Section V concludes with a discussion and summary.

II. THE MODEL

In order to proceed with the multimodal problem we should start from some general discussion of cantilever dynamics.[44,45] If we are interested in studying only flexural modes,

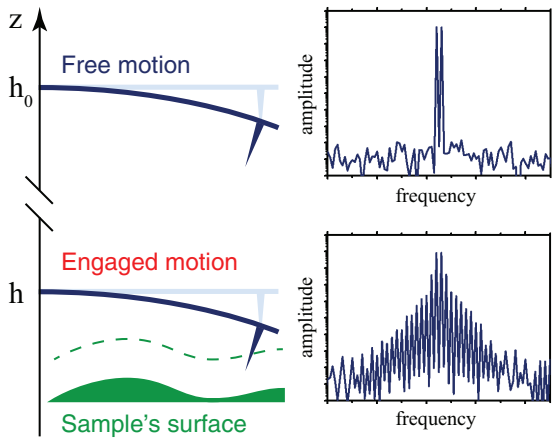

FIG. 1. (Color online) Appearance of new frequencies in the spectrum of the tip motion in ImAFM due to the nonlinearities in the tip-surface interaction. The dashed line shows the characteristic range of the tip-surface force.

one-dimensional Euler-Bernoulli beam theory[46–49] is sufficient. Incorporating torsional modes requires the cantilever to be regarded as a two-dimensional object. Many theories have been developed describing the continuum mechanics of two-dimensional plates.[50–53] A general description of an arbitrary two-dimensional cantilever (Fig. 2) is given by the governing equation

$$(\mathcal{G}_{xy} + \mathcal{G}_t)[w(x,y,t)] = F + \mathrm{f}, \tag{1}$$

with an appropriate set of boundary conditions. Here x and y are the two space coordinates, t is time, $w(x,y,t)$ is the dynamic deflection of the plate normal to the x-y plane of the plate at rest, $\mathcal{G}_{xy}$ is a space coupling operator which corresponds to the two-dimensional mathematical model relating the stresses to the deformations in thin plates, and $\mathcal{G}_t$ is a time evolution operator which represents inertia and damping. F and f are a scalar quantities which are projections onto w, of the two-dimensional vector force field acting on the tip, and the drive, respectively. In general, the projected tip-surface force F can depend explicitly on the deflection w, its velocity $\dot{w}$, past trajectories $\{w,\dot{w}\}|_{-\infty}^{t}$, and time t. In this paper we restrict ourselves to F which are not dependent on past trajectories. We consider only the case of small deflections, so $\mathcal{G}_{xy}$ and $\mathcal{G}_t$ are linear. For example, within the Kirchhoff-Love plate theory[50] the space operator for a homogeneous cantilever reads

$$\mathcal{G}_{xy} := \frac{2h^3 E}{3(1-\nu^2)}\left(\frac{\partial^4}{\partial x^4} + 2\frac{\partial^4}{\partial x^2 \partial y^2} + \frac{\partial^4}{\partial y^4}\right), \tag{2}$$

where $2h$ is the cantilever thickness, E is the Young's modulus, and ν is the Poisson's ratio. The theory assumes that a midsurface plane can be used to represent a three-dimensional plate in a two-dimensional form. The time evolution operator $\mathcal{G}_t$ consists of an inertial term, and for the case of a homogeneous viscous media, a linear damping term

$$\mathcal{G}_t := 2\rho h \frac{\partial^2}{\partial t^2} + 2\gamma \frac{\partial}{\partial t}, \tag{3}$$

where ρ is the cantilever density and γ is a damping coefficient.

The linearity of $\mathcal{G}_{xy}$ and $\mathcal{G}_t$ gives a dynamics of the two-dimensional cantilever which is well approximated by a system of differential equations for the generalized coordinates q_i representing deflections of its normal modes (see the Appendix for a derivation)

$$k_i\left(\frac{1}{\omega_i^2}\ddot{q}_i + \frac{1}{Q_i\omega_i}\dot{q}_i + q_i\right) = F_i(t) + \mathrm{f}_i(t). \tag{4}$$

Here each generalized coordinate q_i has a stiffness k_i, resonant frequency ω_i, and quality factor Q_i. $F_i(t)$ is the projection of the nonlinear tip-surface force and $\mathrm{f}_i(t)$ is the projection of the drive force onto the ith eigenmode. The problem of mapping the eigenmode coordinates q_i onto the physical position of the tip $\mathbf{r} \equiv (z,y)^\intercal$ (hereafter $\intercal$ denotes transpose), as well as the relationship between F_i and the actual vector force field acting on the tip $\mathbf{F}^{\mathrm{ts}}(\mathbf{r},\dot{\mathbf{r}})$, is determined by the cantilever and tip geometry, as briefly discussed in Sec. IV.

III. RECONSTRUCTING FORCE FROM INTERMODULATION WITH MULTIPLE EIGENMODES

We recall the basic steps to get information about the projected tip-surface force F_i in the frequency domain using the intermodulation technique. First, we excite one or several generalized coordinates [Eq. (4)] with the drive f_i and measure its motion spectrum at the height h_0, far from the sample surface, so $F_i|_{h_0} \simeq 0$ for all t. This free oscillation spectrum is denoted

$$\hat{q}_i|_{h_0} = \chi_i \hat{\mathrm{f}}_i, \tag{5}$$

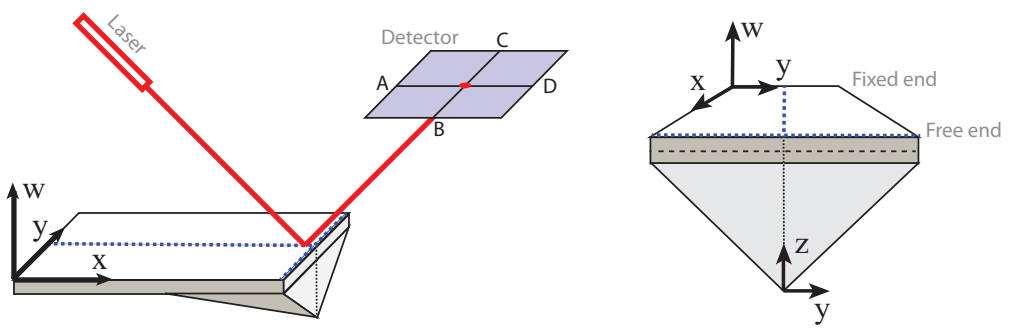

FIG. 2. (Color online) Schematic representation of the two-dimensional cantilever and detection principle in AFM.

where the hat represents the discrete Fourier transform (DFT)

$$\hat{q}(n\delta\omega) \equiv \mathcal{F}[q(t)](n\delta\omega) := \sum_{m=0}^{M-1} q(m\delta t)e^{-2\pi\imath nm/M} \tag{6}$$

of a signal measured M times with an interval δt and the linear response function χ_i is introduced

$$\chi_i(\omega) = k_i^{-1}\left[1 + \frac{\imath}{Q_i}\left(\frac{\omega}{\omega_i}\right) - \left(\frac{\omega}{\omega_i}\right)^2\right]^{-1}. \tag{7}$$

Using pairs of drive tones with the same amplitude A_i which are separated by $\delta\omega$ and placed close to each resonance $n_i\delta\omega < \omega_i < (n_i + 1)\delta\omega$, where n_i is an integer,

$$\mathrm{f}_i(t) = A_i\{\cos(n_i\delta\omega t) + \cos[(n_i + 1)\delta\omega t]\}, \tag{8}$$

we obtain a free, linear response spectrum [Eq. (5)] consisting of components only at the drive frequencies $n_i\delta\omega$ and $(n_i + 1)\delta\omega$ (Fig. 1). Data acquisition in ImAFM should be performed over at least one total period of the drive $T = 2\pi/\delta\omega$ while measuring subsequent periods only improves the SNR of the measured spectra.[54,55]

We then move the cantilever closer to the sample to the engaged height h, so the oscillating tip starts to interact with a surface and measure the motion spectrum again

$$\hat{q}_i|_h = \chi_i(\hat{F}_i + \hat{\mathrm{f}}_i). \tag{9}$$

Finally, the difference between this engaged motion spectrum [Eq. (9)] and free motion spectrum [Eq. (5)] yields the desired interaction force spectrum

$$\hat{F}_i = \chi_i^{-1}\left(\hat{q}_i|_h - \hat{q}_i\big|_{h_0}\right) \equiv \chi_i^{-1}\Delta\hat{q}_i, \tag{10}$$

where the finite difference operator Δ is used for short. Thus, we have obtained information about the projection of the tip-surface force F_i in the frequency space representation of the motion and we are in a position to discuss the reconstruction of its dependence on the generalized coordinates q_i and velocities $\dot{q}_i$.

Under ideal conditions, given the full difference spectrum $\Delta\hat{q}_i$ and corresponding response function χ_i, it is possible to find $F_i(t)$ as the inverse Fourier transform of $\hat{F}_i(\omega)$ and then trivially recover its coordinate dependence $F_i(\{q_i,\dot{q}_i\})$ using the measured motion $q_i(t)$. However, in real experiments this naive approach fails due to the strong frequency dependence of χ_i and the measurement limitations imposed by detection noise. In practice, almost all of the spectrum $\hat{q}_i$ is buried under detector noise except for a narrow band near its resonant frequency where the signal-to-noise ratio (SNR) meets the thermal limit. Usually the number of resolvable spectral components B_i in a band surrounding each eigenmode resonance is limited to a few dozen, depending on the difference frequency $\delta\omega$ and the forces experienced during the interaction. The use of several (N) eigenmodes allows for a larger total number of frequency components $B = \sum_{i=1}^{N} B_i$ for force reconstruction.

Different methods have been elaborated for the single mode reconstruction problem using this limited amount of response in the resonant detection band.[27,28,41–43] Here we develop an extension of the spectral fitting method[27,28,43] for the multimodal problem as it allows for a straightforward generalization without involving any sophisticated concepts.[41] Following the method's main idea, one assumes a tip-surface force in the form of some known model function $\tilde{F}_i(q_1, \ldots, q_N; \mathbf{g})$ with a vector $\mathbf{g} = (g_1, \ldots\ g_P)^\intercal$ of P unknown parameters. Fitting the calculated spectrum $\hat{\tilde{F}}_i(\omega)$ to the measured $\hat{F}_i(\omega)$ [Eq. (10)], we minimize the error function in the frequency domain, in a least-square sense

$$\min_{\mathbf{g}} \hat{e}_i = \hat{F}_i - \hat{\tilde{F}}_i(q_1, \ldots, q_N; \mathbf{g}). \tag{11}$$

The model $\tilde{F}_i$ can be a particular phenomenological expression, for example the van der Waals–Derjagin–Muller–Toporov (vdW-DMT) force[56] or its modifications.[5,57,58] However, in the general case we do not know the exact form of the interaction and should choose some generic function structure, for instance a truncated power series expansion in the following polynomial form:

$$\tilde{F}_i(q_1, \ldots, q_N) = \sum_{i_1=0}^{P_1} \cdots \sum_{i_N=0}^{P_N} g_{i_1\cdots i_N} q_1^{i_1} \cdots q_N^{i_N} = \mathbf{q}^\intercal\mathbf{g}. \tag{12}$$

Here P_i is the degree of the polynomial in q_i, $\mathbf{q}$ and $\mathbf{g}$ are vectors of basis functions and parameters, respectively, each being of size $P = \prod_{i=1}^{N} P_i$,

$$\begin{aligned} \mathbf{q} &= \left(1,\ q_1,\ q_1^2,\ \ldots,\ q_2,\ q_1q_2,\ q_1^2q_2,\ \ldots\right)^\intercal, \\ \mathbf{g} &= \left(g_{00\ldots},\ g_{10\ldots},\ g_{20\ldots},\ \ldots,\ g_{01\ldots},\ g_{11\ldots},\ g_{21\ldots},\ \ldots\right)^\intercal. \end{aligned} \tag{13}$$

Although the polynomial model is more universal, it usually contains a much larger number of unknown parameters[59] which do not directly correspond to physical properties of the material or surface.

Inserting Eq. (12) into Eq. (10), we obtain a system of linear equations for the polynomial coefficients $g_{i_1\ldots i_N}$ which is conveniently represented in matrix notation[60]

$$\mathbf{g} = \hat{\mathbf{H}}^+\hat{\mathbf{F}}_i, \tag{14}$$

where $\hat{\mathbf{H}}$ is a $B \times P$ matrix with rows $\hat{H}_n = \mathcal{F}_n[\mathbf{q}^\intercal]$ (n is the corresponding component of the discrete Fourier transform of $\mathbf{q}$), $\hat{\mathbf{H}}^+$ its Moore-Penrose pseudoinverse, and $\hat{\mathbf{F}}_i$ a vector of size B.[61] Note that total number of unknown parameters P cannot be greater than B and in the case of an overdetermined system ($P < B$) the pseudoinverse will give a unique solution to Eq. (12) in a least-square sense [Eq. (11)]. Reconstruction of the velocity-dependent part of the force F_i can be performed in the same way as for a conservative force, by polynomial expansion in $\dot{q}_i$ with corresponding coefficients.

IV. RECONSTRUCTION OF TIP-SURFACE FORCES FROM MULTIMODAL INTERMODULATION AFM SPECTRA

The reconstruction of tip-surface force from multiple eigenmodes is thus a straightforward generalization of the single eigenmode problem, albeit with the complication of keeping track of multiple modes and the possibility that tones can intermodulate between these modes. From an algebraic point of view the spectral fitting method can be regarded as a multivariate interpolation[62] and the simplest model which is linear in the parameters suffers from Runge's phenomena[63,64] when high-order nonlinearities couple the multiple eigenmode coordinates. Furthermore, reconstruction from many eigenmodes is a multidimensional problem with

many model parameters and it will ultimately suffer from the need to either calibrate or determine these parameters from the limited number of intermodulation products that can be extracted from the narrow frequency bands near the resonances.

In a real experiment, the AFM detector is typically not able measure over a frequency range which covers many eigenmodes of the cantilever. Furthermore, the AFM detector is only capable of measuring two signals, corresponding to two orthogonal motions of the cantilever, that of flexing and twisting. The case of only two eigenmodes is therefore a reasonable simplification of the multimodal problem which is of great practical interest. In the following we restrict ourselves to this bimodal case.

We are interested in reconstruction of the two-dimensional tip-surface vector force field $\mathbf{F}^{\mathrm{ts}}(\mathbf{r},\dot{\mathbf{r}})$ which depends on the physical tip position in the y-z plane, $\mathbf{r} = (z,y)^{\intercal}$. Before we proceed with the two-mode analysis we should map the set of forces F_i acting on the cantilever eigenmodes q_i onto the physical force $\mathbf{F}^{\mathrm{ts}}$. With this aim, we can transform the basis set for defining q_i to separate "pure" modes from "mixed" modes. Applying some coordinate transformation, the exact form of which depends on the geometrical shape of the cantilever, we obtain the pure eigencoordinates z_i and y_i contributing only to the tip position perpendicular and parallel to the surface, respectively. The remaining $\mathbf{q}_i^{\times}$ are mixed eigencoordinates of the cantilever, or cross modes contributing to both coordinates z and y simultaneously, so that

$$z = \sum z_i + \sum \mathbf{q}_i^{\times} \cdot \mathbf{z}, \quad y = \sum y_i + \sum \mathbf{q}_i^{\times} \cdot \mathbf{y}. \tag{15}$$

Here the second terms are projections of the mixed eigencoordinates onto the tip coordinate system $(\mathbf{z},\mathbf{y})$. In doing so, the force $\mathbf{F}^{\mathrm{ts}}$ is projected onto the $(\mathbf{z},\mathbf{y})$ so that its components parallel to the surface F_z and perpendicular to the surface F_y act on the corresponding pure modes, i.e., $F_i = F_z$ for each z_i, $F_i = F_y$ for each y_i, and different force projections act on the mixed modes.

Simultaneous excitation of the several pure eigenmodes coupled by nonlinear tip-surface interaction leads to excitation of the mixed modes which allows for measurements of the response in additional frequency bands. Although it would provide additional information, in this paper we investigate the simplest multimodal motion, that of pure bimodal motion without considering the cross modes. In this case, analysis of the cantilever dynamics reduces to study of two characteristic regimes: bimodal motion of the collinear eigencoordinates (e.g., two flexural or torsional modes) and orthogonal eigencoordinates (one flexural and one torsional mode). Let us proceed with the former.

A. Case 1: Bimodal tip motion in one dimension

This case corresponds to the dynamics of two flexural modes z_1 and z_2, so that the total perpendicular tip deflection $z = z_1 + z_2$,

$$\begin{aligned} k_1\left(\frac{1}{\omega_1^2}\ddot{z}_1 + \frac{1}{Q_1\omega_1}\dot{z}_1 + z_1\right) &= F_z(z,\dot{z}) + \mathrm{f}_1(t), \\ k_2\left(\frac{1}{\omega_2^2}\ddot{z}_2 + \frac{1}{Q_2\omega_2}\dot{z}_2 + z_2\right) &= F_z(z,\dot{z}) + \mathrm{f}_2(t). \end{aligned} \tag{16}$$

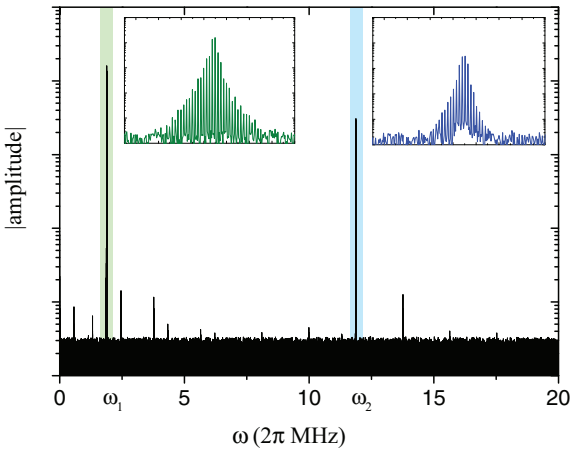

FIG. 3. (Color online) Simulated spectrum of the engaged cantilever motion with two flexural modes. Two peaks are clearly seen above noise level near the resonant frequencies ω_1 and ω_2 which consist of the intermodulation products depicted in insets. The spectrum is obtained by integrating Eq. (16) with the tip-surface force [Eq. (22)] and subsequent addition of white noise.

Here, on the right-hand side, we have the same vector component F_z of the tip-surface force field[65] depending on z and $\dot{z}$.

First, let us consider a model for the position-dependent part of F_z in some general form

$$\tilde{F}_z(z_1,z_2) = \sum_{i=0}^{P_{z_1}} \sum_{j=0}^{P_{z_2}} g_{ij} z_1^i z_2^j. \tag{17}$$

This model requires determination of a large number $P_z(P_z - 1)/2$ of coefficients g_{ij} in order to define the polynomial of order $P_z = P_{z_1} P_{z_2}$. If we use the fact that $F_z(z_1,z_2) = F_z(z_1 + z_2)$ we can define a polynomial of the form

$$\tilde{F}_z(z_1 + z_2) = \sum_{i=0}^{P_z} g_i (z_1 + z_2)^i, \tag{18}$$

which contains only $P_z + 1$ unknown coefficients g_i. In this case we should consider not two separate spectra of dynamic variables $\hat{z}_1$ and $\hat{z}_2$ but one united spectrum $\hat{z} = \hat{z}_1 + \hat{z}_2$ which is actually measured. As a result, it is possible to obtain a tip-surface interaction spectrum $\hat{F}_z$ (Fig. 3),

$$\hat{F}_z = \chi^{-1} \Delta \hat{z}, \tag{19}$$

making use of the total response function[66] $\chi = \chi_1 + \chi_2$ depicted in Fig. 4.

Prior to force reconstruction it is necessary to investigate what kind of information about F_z is contained in the spectral bands for z_1 and z_2. In the current investigation we try to reconstruct the force using information contained only in the narrow frequency bands near ω_1 and ω_2, so all weak response peaks outside these bands are discarded. We also require that the second resonance frequency ω_2 is not an integer multiple of the ω_1, so the second band does not capture any higher harmonics and intermodulation products produced by the drive in the first band. If ω_2 were a harmonic of ω_1 it would be of considerable advantage for force measurement.[67] Considering

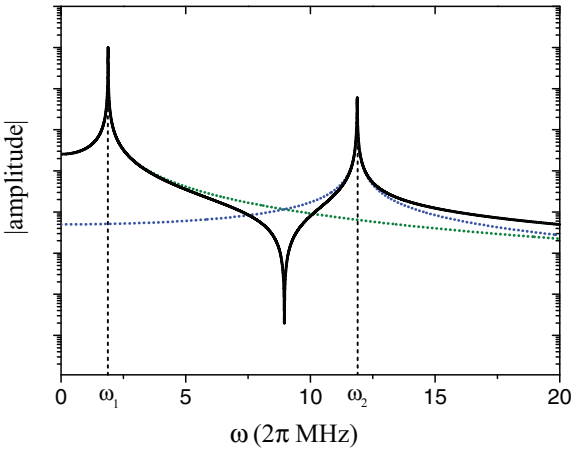

FIG. 4. (Color online) Total transfer function χ (black solid line) for the cantilever with two flexural modes with transfer functions χ_1 and χ_2 (green and blue dotted lines, respectively).

the monomial basis [Eq. (18)] we can approximately evaluate the Fourier spectrum of the ith power $\mathcal{F}[z^i] = \mathcal{F}[z] * \cdots * \mathcal{F}[z]$ via convolution of the transfer function χ with itself, which gives an upper bound of the response in the frequency

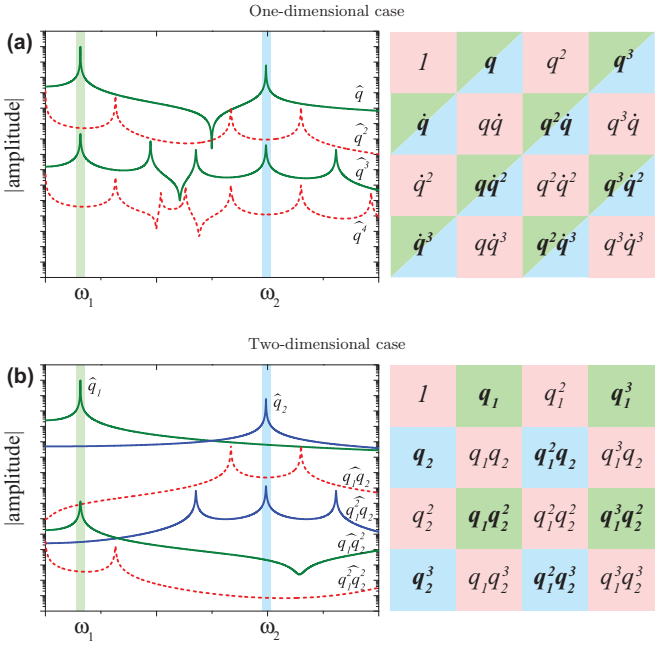

FIG. 5. (Color online) (a) Response spectra for powers of a single dynamic variable with two resonances and (b) two separate variables, each with one resonance. Two frequency windows near resonances ω_1 and ω_2 are highlighted with light green and blue colors, respectively. Red dashed line means that the corresponding maximum response lies outside the frequency bands. Tables on the right indicate how dynamical variable combinations contribute to the corresponding narrow spectral bands: almost no contribution (red), maximum contribution into the first band (light green), second band (light blue), or both bands.

domain. Figure 5(a) demonstrates that only components with odd powers i have significant value in the narrow bands near the resonances. Consequentially, only parameters g_i for odd powers z^i (i odd) can be found directly using the measured spectrum. Although two flexural modes give us twice the number of spectral components in comparison with single mode case, the addition of a second mode does not provide any additional information. The reason being that in both cases of one- and two-dimensional tip motion, the measured spectrum in the narrow bands near resonances consists of convolutions of motion spectra of two corresponding degrees of freedom $\mathcal{F}[q_1^i] * \mathcal{F}[q_2^j]$. However, in the one-dimensional case a force depends on the sum coordinate, i.e., $F(z,\dot{z})$, where $z = z_1 + z_2$, which leads to equal information about the force in both bands. This is in contrast to the two-dimensional case, where the force has a separate dependence on each coordinate z and y.

Having solved the system for the odd parameters, we can use them to recover the even parameters by applying an additional constraint: That the tip-surface force for tip positions above its rest point approximately equals zero[60] $F_z(z > 0) \approx 0$, which leads to the system of equations at all measured times t_i when $z_i \equiv z(t_i) > 0$,

$$\mathbf{Z}^{\text{even}}\mathbf{g}^{\text{even}} = -\mathbf{Z}^{\text{odd}}\mathbf{g}^{\text{odd}}, \tag{20}$$

where $\mathbf{g}^{\text{even}} = (g_0, g_2, \ldots, g_{P_z-1})^{\mathsf{T}}$, $\mathbf{g}^{\text{odd}} = (g_1, g_3, \ldots, g_{P_z})^{\mathsf{T}}$, and $\mathbf{Z}^{\text{even}}$ and $\mathbf{Z}^{\text{odd}}$ are matrices with elements $z_{ij}^{\text{even}} = z_i^{2j}$ and $z_{ij}^{\text{odd}} = z_i^{2j+1}$ respectively.

Reconstruction of the velocity-dependent part of F_z is achieved by adding a new variable $\dot{z} = \dot{z}_1 + \dot{z}_2$ to the model [Eq. (18)] which consequently increases the number of parameters by the degree of the polynomial in $\dot{z}$,

$$\tilde{F}_z(z,\dot{z}) = \sum_{i=0}^{P_z}\sum_{j=0}^{P_{\dot{z}}} g_{ij} z^i \dot{z}^j. \tag{21}$$

Since $\mathcal{F}[z^i\dot{z}^j] \propto \mathcal{F}[z^{i+j}]$, only coefficients g_{ij} in front of $z^i\dot{z}^j$ where $i + j$ is odd can be determined from the measured spectrum. While coefficients before $z\dot{z}$, $z^3\dot{z}$, $z\dot{z}^3$, etc. can be found using Eq. (20).

We simulate the one-dimensional bimodal case using the CVODE integrator[68] with $\omega_1 = 2\pi$ 300 kHz, $k_1 = 40$ N/m, $Q_1 = 400$, $\omega_2 = 6.3\omega_1$, $k_2 = 50k_1$, $Q_2 = 3Q_1$ (ratios for the second mode are taken from Ref. 69). The driving forces $f_{1,2}$ are chosen to have the same phase and give equal maximum free response (when $F_z \equiv 0$) at each mode $A_{z_1} = A_{z_2} = 12.5$ nm so the total maximum amplitude of oscillations is $A_z = 25$ nm; all four drive frequencies $\omega_{1,2} \pm \delta\omega/2$ are integer multiples of a base frequency $\delta\omega = 2\pi$ 0.2 kHz. The engaged height h above the surface is 17 nm. The model of the tip-surface force F_z is the vdW-DMT force[56] with the nonlinear damping term exponentially dependent on the tip position

$$\begin{aligned} F_z(z,\dot{z}) &= F_z^{\text{con}}(z) + F_z^{\text{dis}}(z,\dot{z}). \\ F_z^{\text{con}}(z) &= \begin{cases} -\frac{HR}{6(z+h)^2}, & z+h \geqslant a_0, \\ -\frac{HR}{6a_0^2} + \frac{4}{3}E^*\sqrt{R[a_0-(z+h)]}, & z+h < a_0, \end{cases} \\ F_z^{\text{dis}}(z,\dot{z}) &= -(\gamma_1\dot{z} + \gamma_3\dot{z}^3)e^{-(z+h)/\lambda_z}, \end{aligned} \tag{22}$$

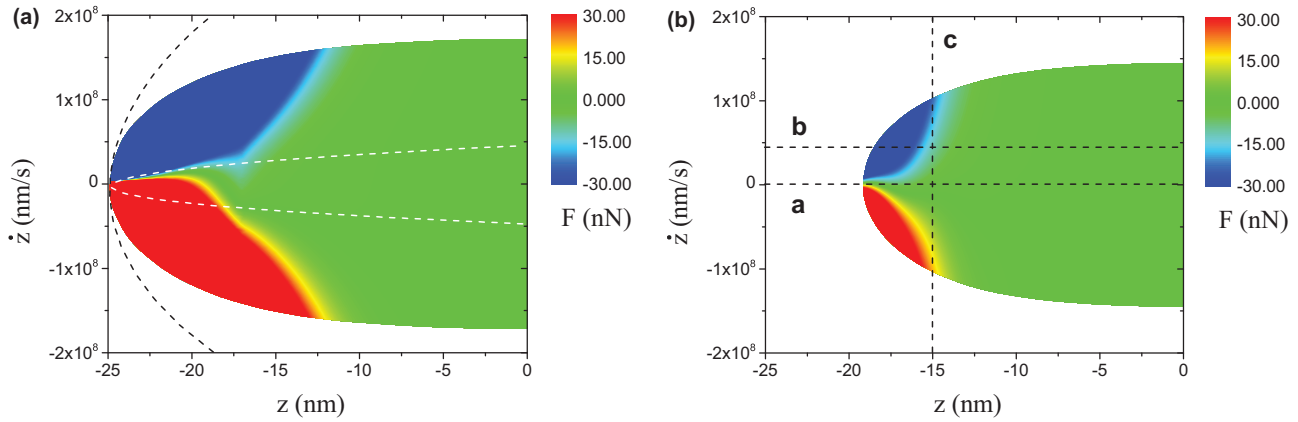

FIG. 6. (Color online) (a) The actual vdW-DMT force with position dependent damping used in the simulation shown for the region of the free tip motion with bimodal drive of fixed total amplitude ($A_1 + A_2 = 25$ nm). White and black dashed lines circumscribe the regions of phase space for single mode drive of the first and second modes, respectively, with amplitude 25 nm (difference between maximum velocities is about an order of magnitude). (b) Reconstructed force shown in the region of the engaged tip motion. Cross sections (a)–(c) are depicted in Figs. 7(a)–7(c) to highlight agreement between the actual force used in simulation and the reconstructed force.

with the following seven phenomenological parameters: intermolecular distance $a_0 = 0.3$ nm, Hamaker constant $H = 7.1 \times 10^{-20}$ J, effective modulus $E^* = 1.0$ GPa, tip radius $R = 10$ nm, damping decay length $\lambda_z = 1.5$ nm, and damping factors $\gamma_1 = 2.2 \times 10^{-7}$ kg/s and $\gamma_3 = 10^{-22}$ kg s/m^2 [Fig. 6(a)]. It is worth noting that the calibration of the second eigenmode parameters ω_2, Q_2, and k_2 which are required for force reconstruction as well as optical lever responsivity,[70] is itself a challenging task in multimodal AFM.[69,71,72]

Numerical results show that the force reconstruction using higher powers of $\dot{z}^j$ ($j > 1$) is less reliable as it encounters two principal difficulties: (i) In order to find a larger number of parameters g_{ij}, a larger number of the intermodulation peaks with lower SNR should be used because the second band does not bring new information about nonlinear forces; and (ii) there is a lack of information needed to restore the additional coefficients g_{ij} ($i + j$ even) in Eq. (21), as we do not have a constraint on $\dot{z}$ dependence analogous to Eq. (20). Therefore, we do not reconstruct the nonlinear (nonviscous) part of the dissipative force [Eq. (22)] and restrict the model [Eq. (21)] to be linear in $\dot{z}$ ($P_{\dot{z}} = 1$).

Using $B_{1,2} = 24$ peaks in each band (Fig. 3) for the reconstruction, we assume the model degree in z [Eq. (21)] to be $P_z = 21$. This numerical analysis suggests that there is no difference in the quality of the reconstructed force using intermodulation products from frequency bands surrounding the first, second, or both resonances. We show results for the reconstructed $\tilde{F}_z(z,\dot{z})$ and its cross sections in Figs. 6(b) and 7 using only the resonant detection band around the first eigenmode. The linear fit [Eq. (21)] for the model with nonlinear damping [Eq. (22)] nicely captures the overall trend of the dissipative part and the reconstructed conservative part demonstrates excellent agreement with the actual force. If we simulate Eq. (16) using the force F_z linear in $\dot{z}$, for instance assuming $\gamma_3 = 0$ in Eq. (22), the reconstructed force $\tilde{F}_z$ shows nearly perfect agreement with the actual force F_z (figures are not included).

One can compare the information contained in the two frequency bands near each eigenmode resonance by estimating the quality of the reconstruction as a function of the number

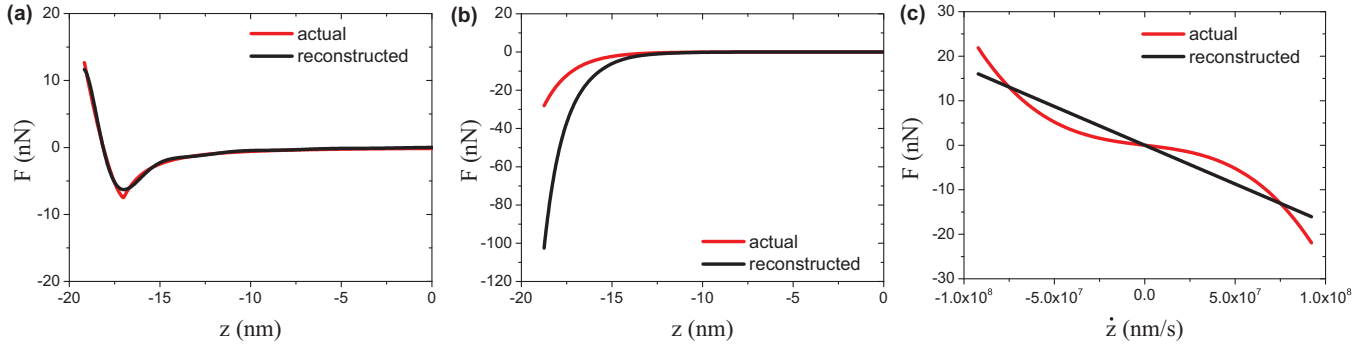

FIG. 7. (Color online) Cross sections of the reconstructed tip-surface force (black) with comparison to the actual force used in simulation (red) for the cantilever driven at two flexural modes (z_1 and z_2). (a) $\tilde{F}_z(z,\dot{z}=0)$; (b) $\tilde{F}_z(z,\dot{z}=0.2\dot{z}_{\max}) - \tilde{F}_z(z,\dot{z}=0)$; and (c) $\tilde{F}_z(z = 0.75z_{\min},\dot{z})$. The linear fit for nonlinear damping nicely recovers the overall trend and the conservative part shows excellent agreement with the actual force.

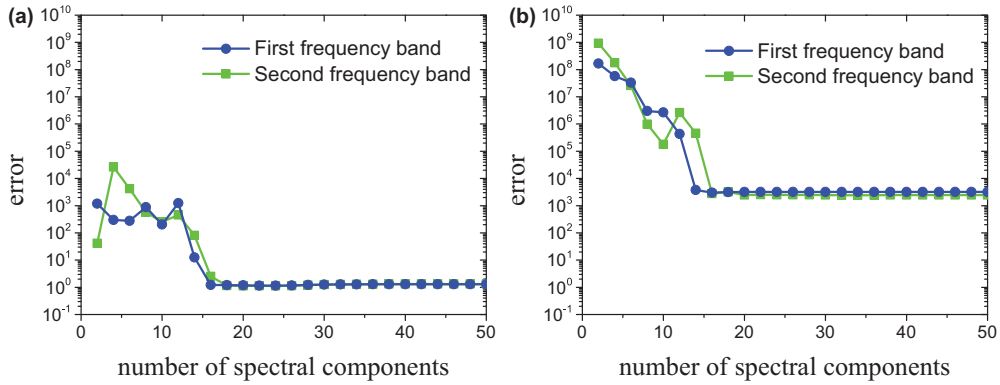

FIG. 8. (Color online) Absolute error of the reconstruction of (a) conservative part of the tip-surface force [Fig. 7(a)] and (b) dissipative part [Fig. 7(b)] versus number of spectral components taken into account in the first frequency band (blue circles) and in the second (green squares).

of spectral components $B_{1,2}$ used in the reconstruction, as the least-square error function

$$e_i(B_i) = \int_{z_{\min}}^{z_{\max}} [\tilde{F}_z(z,\dot{z}|B_i) - F_z(z,\dot{z})]^2 dz. \tag{23}$$

This error function is plotted versus the number of spectral components in Fig. 8. We see similar behavior for both bands: Significant drop in the error for the number of spectral components larger than half of the polynomial power $P_z = 21$ in the expansion of $\tilde{F}_z$, and no quantitative improvements for a larger number of spectral components.

Another interesting observation regards the reconstruction of a dissipative force which turns-on only for the tip velocities $\dot{z}$, higher than the maximum velocity of the first mode z_1 (for some constant amplitude) and is zero otherwise. Information from both bands gives approximately the same reconstructed curves showing the overall trend of the dissipative part and in excellent agreement for the conservative part (plots not shown). However, reconstructing with spectral components from only the first frequency band yields more accurate dissipative force approximation as z_1 has smaller stored oscillation energy and, consequently, is more vulnerable to the dissipative force than z_2. Nonetheless, if we excited only the first mode, we would not be able to reconstruct this "threshold" dissipative force at all, as the magnitude of the tip velocity would not be enough to turn on the dissipation. Thus, simultaneous excitation of two eigenmodes allows one to explore a wider region of the phase space of the tip motion [Fig. 6(a)] while keeping the total maximum amplitude constant.

B. Case 2: Bimodal tip motion in two dimensions

This case corresponds to the dynamics of one flexural z and one torsional y mode

$$\begin{aligned} k_z\left(\frac{1}{\omega_z^2}\ddot{z} + \frac{1}{Q_z\omega_z}\dot{z} + z\right) &= F_z(z,y) + \mathrm{f}_z(t), \\ k_y\left(\frac{1}{\omega_y^2}\ddot{y} + \frac{1}{Q_y\omega_y}\dot{y} + y\right) &= F_y(z,y) + \mathrm{f}_y(t), \end{aligned} \tag{24}$$

with two different projections of the conservative tip-surface force, F_z and F_y on the right-hand side.

We start from the polynomial models for reconstruction

$$\begin{aligned} \tilde{F}_z(z,y) &= \sum_{i=0}^{P_z}\sum_{j=0}^{P_y} g_{ij}^{(z)} z^i y^j, \\ \tilde{F}_y(z,y) &= \sum_{i=0}^{P_z}\sum_{j=0}^{P_y} g_{ij}^{(y)} z^i y^j. \end{aligned} \tag{25}$$

As for the previous case it is not possible to find all parameters of these models. We are limited in the number of measurable intermodulation products and therefore in the maximum degree of the polynomial. Therefore, we choose the z direction as the most interesting degree of freedom, by which we mean that the maximum degree of the polynomial in this variable will be much higher than for y. In accordance to Fig. 5(b), the information captured about the force F_z will be odd in z and even in y and vice versa for F_y,

$$\tilde{F}_z(-z,\pm y) = -\tilde{F}_z(z,y), \quad \tilde{F}_y(\pm z,-y) = -\tilde{F}_y(z,y) \tag{26}$$

as the first flexural resonance ω_z is typically far lower in frequency than the first torsional resonance ω_y.[44] It is possible to recover the coefficients $g_{ij}^{(z)}$ of even powers of y and $g_{ij}^{(y)}$ of odd powers of y (when $i + j$ is even) by using the additional constraint for the z dependence of the force components $F_{z,y}(z > 0, y) \approx 0$ and Eq. (20). While the information about all coefficients of $\tilde{F}_z$ with odd powers of y and $\tilde{F}_y$ with even powers of y is lost because we have no such constraint on the y dependence.

The simulation parameters for Eq. (24) are $\omega_z = 2\pi\ 300$ kHz, $k_z = 40$ N/m, $Q_z = 400$, $\omega_y = 6.3\omega_z$, $k_y = 50k_z$, $Q_y = 3Q_z$. The driving forces $\mathrm{f}_{z,y}$ are chosen to have the same phase and give maximum free response (when $F_{z,y} \equiv 0$) $A_z = 25$ nm and $A_y = 12.5$ nm; all four drive frequencies $\omega_{z,y} \pm \delta\omega/2$ are integer multiples of base frequency $\delta\omega = 2\pi\ 0.2$ kHz. The engaged height h above the surface is 17 nm. The model for the component of the tip-surface force perpendicular to the surface F_z is the same vdW-DMT force [Eq. (22)] used in the previous case, without the dissipation term F_z^{dis}. The model of the force component parallel to the surface is a nonlinear conservative restoring force

$$F_y(z,y) = -(c_1 y + c_3 y^3)e^{-(z+h)/\lambda_z}, \tag{27}$$

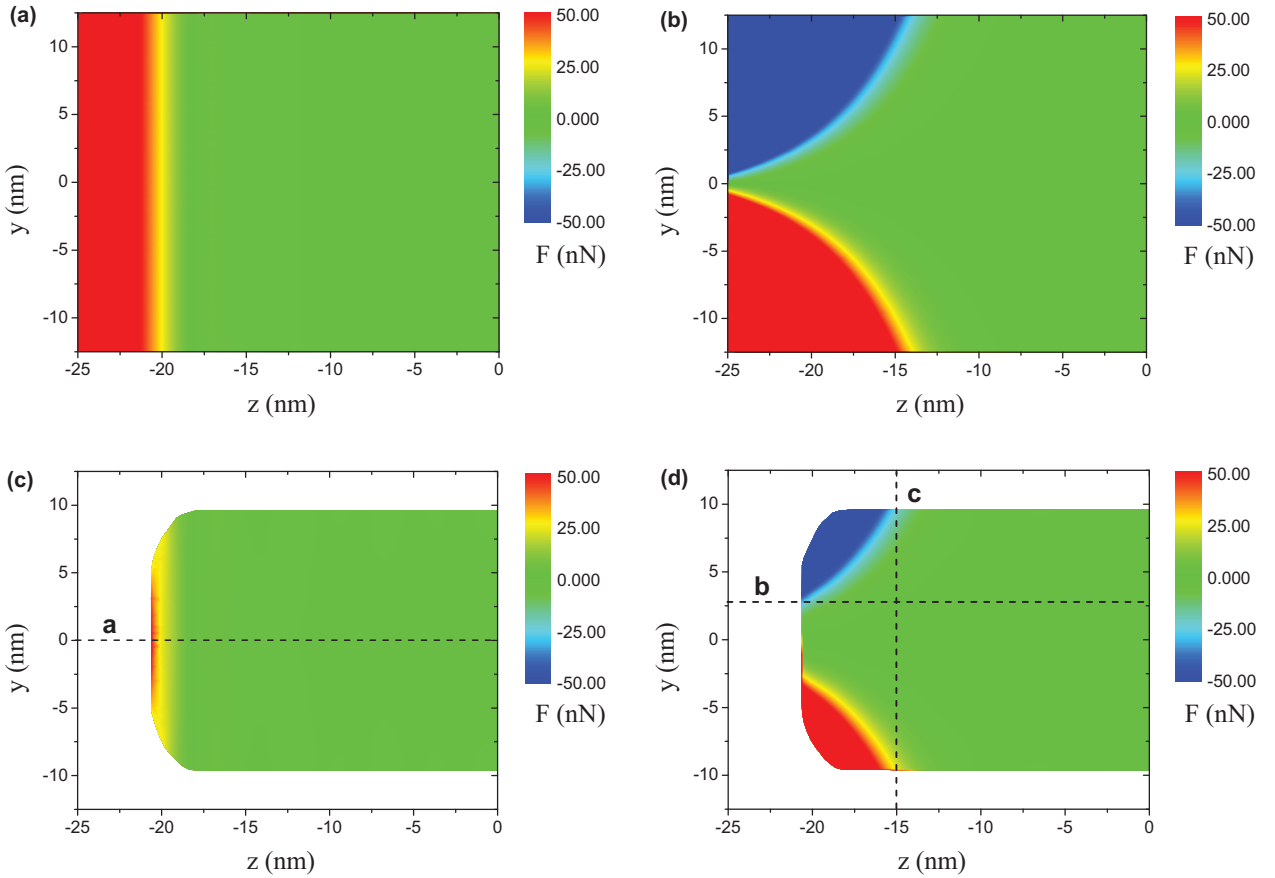

FIG. 9. (Color online) Components F_z and F_y of actual two-dimensional conservative force used in the simulation shown for the region of the free tip motion [(a) and (b)] and reconstructed components shown in the region of the engaged tip motion [(c) and (d)]. Cross-sections (a)–(c) are illustrated in Figs. 10(a)–10(c) to highlight agreement between the actual force used in simulation and the reconstructed force.

where $\lambda_z = 1.5$ nm, $c_1 = 0.22$ N/m, and $c_3 = 0.1$ N/m^3 are constants. These two components of $\mathbf{F}^{\rm ts}(\mathbf{r})$ are illustrated in Figs. 9(a) and 9(b).

Using only 24 intermodulation peaks in each band for $\hat{z}$ and $\hat{y}$, the spectral fitting method reconstructs the two-dimensional vector force field $\mathbf{F}^{\rm ts}$ defined by Eqs. (22) and (27) up to the 21st power in z and third power in y [Figs. 9(c), 9(d), and 10]. The reconstructed force is in good agreement with the actual model near the surface and perfect agreement is reachable if we assume the model for $\tilde{F}_z$ as Eq. (25), only independent of y.

V. CONCLUDING REMARKS

In this paper we discussed the basic problem of multimodal AFM and we proposed a theoretical framework for

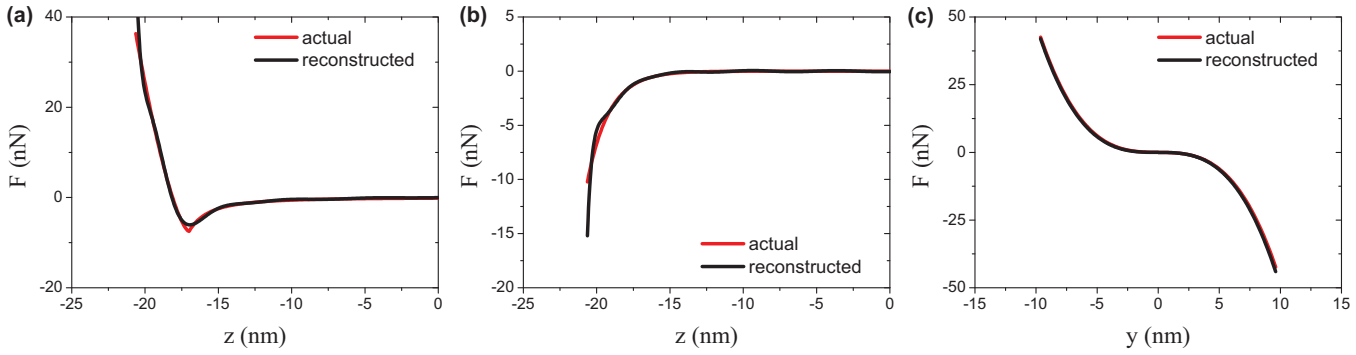

FIG. 10. (Color online) Cross sections of reconstructed tip-surface force (black) with comparison to the actual force used in simulation (red) for the cantilever driven at one flexural and one torsional mode (z and y). (a) $\tilde{F}_z(z)$; (b) $\tilde{F}_y(z, y = 0.2\dot{z}_{\rm max})$; and (c) $\tilde{F}_y(z = 0.75z_{\rm min}, y)$. The reconstructed force is in good agreement with the actual force near the surface. Perfect agreement is reachable if we assume model for F_z independent of y.

reconstructing forces using the ImAFM technique. We demonstrated the possibility of reconstructing tip-surface forces for two characteristic bimodal cases. A crucial difference between them was found: Measurement of response at the additional eigenmode provides new information only in the case where the force cannot be represented as a linear combination of the two degrees of freedom, i.e., $F(q_1,q_2) \neq F(q_1+q_2)$. This type of force is experienced by a tip interacting with a surface when the cantilever is undergoing two-dimensional motion, for example when the cantilever is excited at one torsional and one flexural eigenmode. We studied such interaction and found that we could reconstruct conservative forces which contained the most nonlinear behavior in the first degree of freedom, and are linear or cubic in the second degree of freedom.

For the case of one-dimensional motion, e.g., two flexural modes where $F(q_1,q_2) = F(q_1+q_2)$, we found that excitation of two modes with two well-separated resonances does not allow for a precise reconstruction of a nonlinear damping force using only the information contained in the narrow bands near each resonance. However, the reconstruction using response in only one band nicely captures the linear part, or that of viscous damping. While the use of a higher frequency flexural eigenmode does not in principle provide any new information, it does allow for force reconstruction in a wider region of phase space of the tip motion, enabling exploration of dissipative interactions inaccessible to the first mode alone for a given maximum amplitude of motion. We also found that the lower frequency flexural eigenmode was more sensitive to dissipative tip-surface forces.

From the analysis presented here we conclude that bimodal AFM offers a significant advantage when one simultaneously excites and measures response near two eigenmodes separating orthogonal directions of tip motion. In this case, bimodal AFM allows for simultaneous reconstruction of both vertical and lateral forces and it represents a path toward the determination of vectorial tip-surface force fields by frequency domain multiplexing of the response of an AFM cantilever.

ACKNOWLEDGMENTS

This work is supported by Nordita, DOE, VR VCB 621-2012-2983, the Knut and Allice Wallenberg Foundation, and the Olle Enqvist Foundation.

APPENDIX: GENERALIZED EIGENCOORDINATES

We start from the governing equation for a two-dimensional cantilever,

$$(\mathcal{G}_{xy} + \mathcal{G}_t)[w(x,y,t)] = F(x,y,t) \tag{A1}$$

and try to find solution $w(x,y,t)$ separated in time and space, and expanded into the set of normal modes

$$w(x,y,t) = \sum_{i=0}^{\infty} \phi_i(x,y) q_i(t). \tag{A2}$$

Functions ϕ_i form orthonormal set on the geometrical shape of cantilever Ω_c,

$$\int_{\Omega_c} \phi_i \phi_j \, d\Omega = \delta_i^j, \tag{A3}$$

where $d\Omega \equiv dx\,dy$ and δ_i^j is the Kronecker δ.

Inserting solution [Eq. (A2)] into Eq. (A1) with the following multiplication by ϕ_i and integration over the plane Ω_c yields a system of differential equations for the generalized coordinates $q_i(t)$,

$$q_i \int_{\Omega_c} \phi_i \mathcal{G}_{xy} \phi_i \, d\Omega + \mathcal{G}_t[q_i] \int_{\Omega_c} \phi_i^2 \, d\Omega = \int_{\Omega_c} F(x,y,t) \phi_i \, d\Omega, \tag{A4}$$

here the orthonormal condition [Eq. (A3)] is used.

Denoting $\mathcal{G}_i$ as a differential operator governing motion of the ith generalized coordinate

$$\mathcal{G}_i = k_i + m_i \mathcal{G}_t, \tag{A5}$$

where

$$k_i \equiv \int_{\Omega_c} \phi_i \mathcal{G}_{xy} \phi_i \, d\Omega, \quad m_i \equiv \int_{\Omega_c} \phi_i^2 \, d\Omega \tag{A6}$$

are the effective stiffness and mass of the corresponding degree of freedom, and considering damping and inertia

$$\mathcal{G}_t := \frac{\partial^2}{\partial t^2} + \gamma \frac{\partial}{\partial t}, \tag{A7}$$

with some constant γ (homogeneous viscous medium damping), we arrive at the final system

$$k_i \left(\frac{1}{\omega_i^2} \ddot{q}_i + \frac{1}{Q_i \omega_i} \dot{q}_i + q_i \right) = F_i(t) + \mathrm{f}_i(t), \tag{A8}$$

where the resonant frequencies $\omega_i = \sqrt{k_i/m_i}$ and quality factors $Q_i = \omega_i/\gamma$ are introduced. Here the time-dependent forces

$$F_i(t) + \mathrm{f}_i(t) := \int_{\Omega_c} \phi_i(x,y) F(x,y,t) \, d\Omega \tag{A9}$$

represent contributions of the tip-surface interaction and drive, respectively.

*borysov@kth.se

[1] G. Binnig, C. F. Quate, and C. Gerber, Phys. Rev. Lett. **56**, 930 (1986).
[2] N. A. Burnham, R. J. Colton, and H. M. Pollock, Nanotechnology **4**, 64 (1993).
[3] H.-J. Butt, B. Cappella, and M. Kappl, Surf. Sci. Rep. **59**, 1 (2005).
[4] P. M. Hoffmann, S. Jeffery, J. B. Pethica, H. Ö. Özgür Özer, and A. Oral, Phys. Rev. Lett. **87**, 265502 (2001).
[5] R. García, C. J. Gómez, N. F. Martinez, S. Patil, C. Dietz, and R. Magerle, Phys. Rev. Lett. **97**, 016103 (2006).
[6] C. Negri, N. Manini, A. Vanossi, G. E. Santoro, and E. Tosatti, Phys. Rev. B **81**, 045417 (2010).

[7] K. Saitoh, K. Hayashi, Y. Shibayama, and K. Shirahama, Phys. Rev. Lett. **105**, 236103 (2010).

[8] J.-H. She and A. V. Balatsky, Phys. Rev. Lett. **108**, 136101 (2012).

[9] H. U. Krotil, T. Stifter, H. Waschipky, K. Weishaupt, S. Hild, and O. Marti, Surf. Interface Anal. **27**, 336 (1999).

[10] R. García and R. Perez, Surf. Sci. Rep. **47**, 197 (2002).

[11] F. J. Giessibl, Rev. Mod. Phys. **75**, 949 (2003).

[12] J. E. Sader, T. Uchihashi, M. J. Higgins, A. Farrell, Y. Nakayama, and S. P. Jarvis, Nanotechnology **16**, 94 (2005).

[13] B. J. Albers, T. C. Schwendemann, M. Z. Baykara, N. Pilet, M. Liebmann, E. I. Altman, and U. D. Schwarz, Nanotechnology **20**, 264002 (2009).

[14] L. Gross, F. Mohn, N. Moll, P. Liljeroth, and G. Meyer, Science **325**, 1110 (2009).

[15] S. D. Solares and G. Chawla, J. Appl. Phys. **108**, 054901 (2010).

[16] T. R. Albrecht, P. Grutter, D. Horne, and D. Rugar, J. Appl. Phys. **69**, 668 (1991).

[17] M. Stark, R. W. Stark, W. M. Heckl, and R. Guckenberger, Proc. Natl. Acad. Sci. USA **99**, 8473 (2002).

[18] J. Legleiter, M. Park, B. Cusick, and T. Kowalewski, Proc. Natl. Acad. Sci. USA **103**, 4813 (2006).

[19] M. Lee and W. Jhe, Phys. Rev. Lett. **97**, 036104 (2006).

[20] S. Jesse, S. V. Kalinin, R. Proksch, A. P. Baddorf, and B. J. Rodriguez, Nanotechnology **18**, 435503 (2007).

[21] O. Sahin, S. Magonov, C. Su, C. F. Quate, and O. Solgaard, Nat. Nanotechnol. **2**, 507 (2007).

[22] B. J. Rodriguez, C. Callahan, S. V. Kalinin, and R. Proksch, Nanotechnology **18**, 475504 (2007).

[23] A. Labuda, Y. Miyahara, L. Cockins, and P. H. Grütter, Phys. Rev. B **84**, 125433 (2011).

[24] A. F. Sarioglu, S. Magonov, and O. Solgaard, Appl. Phys. Lett. **100**, 053109 (2012).

[25] M. Serra-García, F. Pérez-Murano, and A. San Paulo, Phys. Rev. B **85**, 035433 (2012).

[26] D. Platz, E. A. Tholén, D. Pesen, and D. B. Haviland, Appl. Phys. Lett. **92**, 153106 (2008).

[27] C. Hutter, D. Platz, E. A. Tholén, T. H. Hansson, and D. B. Haviland, Phys. Rev. Lett. **104**, 050801 (2010).

[28] D. Forchheimer, D. Platz, E. A. Tholén, and D. B. Haviland, Phys. Rev. B **85**, 195449 (2012).

[29] H. Helmholtz, *Sensations of Tone* (Logmans Green and Co., New York, 1895).

[30] R. W. Stark and W. M. Heckl, Surf. Sci. **457**, 219 (2000).

[31] R. Proksch, Appl. Phys. Lett. **89**, 113121 (2006).

[32] N. F. Martinez, S. Patil, J. R. Lozano, and R. García, Appl. Phys. Lett. **89**, 153115 (2006).

[33] D. Rupp, U. Rabe, S. Hirsekorn, and W. Arnold, J. Phys. D: Appl. Phys. **40**, 7136 (2007).

[34] J. R. Lozano and R. García, Phys. Rev. Lett. **100**, 076102 (2008).

[35] J. R. Lozano and R. Garcia, Phys. Rev. B **79**, 014110 (2009).

[36] D. Martinez-Martin, E. T. Herruzo, C. Dietz, J. Gomez-Herrero, and R. García, Phys. Rev. Lett. **106**, 198101 (2011).

[37] A. Yurtsever, A. M. Gigler, and R. W. Stark, J. Phys.: Conf. Ser. **100**, 052033 (2008).

[38] T. Hakari, H. Sekiguchi, T. Osada, K. Kishimoto, R. Afrin, and A. Ikai, Cytoskeleton **68**, 628 (2011).

[39] D. S. Bulgarevich, K. Mitsui, and H. Arakawa, J. Phys.: Conf. Ser. **61**, 170 (2007).

[40] A. M. Gigler, C. Dietz, M. Baumann, N. F. Martinez, R. García, and R. W. Stark, Beilstein J. Nanotechnol. **3**, 456 (2012).

[41] D. Platz, D. Forchheimer, E. A. Tholén, and D. B. Haviland, Nat. Commun. **4**, 1360 (2013).

[42] D. Platz, D. Forchheimer, E. A. Tholén, and D. B. Haviland, Beilstein J. Nanotechnol. **4**, 45 (2013).

[43] D. Platz, D. Forchheimer, E. A. Tholén, and D. B. Haviland, Beilstein J. Nanotechnol. **4**, 352 (2013).

[44] A. Raman, J. Melcher, and R. Tung, Nano Today **3**, 20 (2008).

[45] U. Rabe, K. Janser, and W. Arnold, Rev. Sci. Instrum. **67**, 3281 (1996).

[46] S. I. Lee, S. W. Howell, A. Raman, and R. Reifenberger, Phys. Rev. B **66**, 115409 (2002).

[47] T. R. Rodriguez and R. García, Appl. Phys. Lett. **80**, 1646 (2002).

[48] J. Melcher, S. Hu, and A. Raman, Appl. Phys. Lett. **91**, 053101 (2007).

[49] J. E. Sader, J. Appl. Phys. **84**, 64 (1998).

[50] A. E. H. Love, Philos. Trans. R. Soc. London Sect. A **17**, 491 (1888).

[51] S. Timoshenko and S. Woinowsky-Krieger, *Theory of Plates and Shells* (McGraw-Hill, New York, 1959).

[52] J. N. Reddy, *Theory and Analysis of Elastic Plates and Shells* (CRC, Taylor and Francis, London, 2007).

[53] E. Reissner and M. Stein, *Torsion and Transverse Bending of Cantilever Plates*, Tech. Rep. 2369 (National Advisory Committee for Aeronautics, Washington, D.C., 1951).

[54] E. A. Tholén, D. Platz, D. Forchheimer, M. O. Tholén, C. Hutter, and D. B. Haviland, Rev. Sci. Instrum. **82**, 026109 (2011).

[55] http://intermodulation-products.com.

[56] B. V. Derjaguin, V. M. Muller, and Y. P. Toporov, J. Colloid Interface Sci. **53**, 314 (1975).

[57] B. Gotsmann, C. Seidel, B. Anczykowski, and H. Fuchs, Phys. Rev. B **60**, 11051 (1999).

[58] J. Melcher, S. Hu, and A. Raman, Rev. Sci. Instrum. **79**, 061301 (2008).

[59] Contrary to the model [Eq. (12)], one might consider a model which at first glance appears more suitable, where the force is in the form of a product of single variable polynomials $\tilde{F}_i(q_1,\ldots,q_N) = \prod_{m=1}^{N} P_m(q_m)$. While this model has a much smaller total number of parameters to determine, upon insertion into Eq. (11) we encounter two principal difficulties: (i) If we explicitly perform multiplication and then take the Fourier transform, we obtain a system for the unknown parameters which is nonlinear in the parameters; and (ii) if we insert it as it is, the deconvolution problem must be solved $\hat{F}_i = \hat{P}_1 * \cdots * \hat{P}_N$ which requires knowledge of the spectral components outside narrow bands surrounding resonances.

[60] D. Platz, D. Forchheimer, E. A. Tholén, and D. B. Haviland, Nanotechnology **23**, 265705 (2012).

[61] Strictly speaking, the size of the system is $2B_i$ as the Fourier transform of a real function is symmetrical with respect to the zero frequency but complex conjugated. However, this fact does not provide any additional information and can be used only for improving numerical stability of calculations. Solving this system separately for real and imaginary parts gives the same value of $\mathbf{g}$.

[62] K. Jetter, M. Buhmann, W. Haussmann, R. Schaback, and J. Stoeckler (Eds.), *Topics in Multivariate Approximation and Interpolation*, Studies in Computational Mathematics, Vol. 12 (Elsevier Science, New York, 2006).

[63] C. Runge, Z. Math. Phys. **46**, 224 (1901).

[64] G. Dahlquist and A. Björk, in *Numerical Methods*, Dover Books on Mathematics (Dover, New York, 1974), Sec. 4.3.4, pp. 101–103.

[65]We assume that the tip-surface force acts in a small joint area between the tip and plate. Thus, for a number of the lowest flexural eigenmodes, its contribution in Eq. (A9) can be approximated as $F_i(x,t) = \delta(x - x^{\text{tip}})F_z(t)$. Then Eq. (A8) can be shown to have the same form with the renormalized stiffness $k_i^{\text{corrected}} = \phi_i^{-1}(x^{\text{tip}})k_i$ and the same tip-surface force F_z on the right-hand side.

[66]In principle, it can be generalized for case of N collinear modes $\chi = \sum_{i=0}^{N} \chi_i$.

[67]O. Sahin, G. Yaralioglu, R. Grow, S. F. Zappe, A. Atalar, C. Quate, and O. Solgaard, Sens. Actuators A **114**, 183 (2004).

[68]A. C. Hindmarsh, P. N. Brown, K. E. Grant, S. L. Lee, R. Serban, D. E. Shumaker, and C. S. Woodward, Trans. Math. Software **31**, 363 (2005).

[69]J. R. Lozano, D. Kiracofe, J. Melcher, R. García, and A. Raman, Nanotechnology **21**, 465502 (2010).

[70]The optical lever responsivity α_i is the linear coefficient relating the measured voltage to the eigencoordinate $q_i = \alpha_i V$. In principle this responsivity is different for each eigenmode, as it depends on the mean slope of the cantilever over the area illuminated by the laser spot in the optical detection system.

[71]C. P. Green, H. Lioe, J. P. Cleveland, R. Proksch, P. Mulvaney, and J. E. Sader, Rev. Sci. Instrum. **75**, 1988 (2004).

[72]A. Feiler, P. Attard, and I. Larson, Rev. Sci. Instrum. **71**, 2746 (2000).